IOP Conf. Series: Materials Science and Engineering **328** (2018) 012016 doi:10.1088/1757-899X/328/1/012016

The Effects of Sn Addition on the Microstructure and Surface Properties of Laser Deposited Al-Si-Sn Coatings on ASTM A29 Steel

Olawale S. Fatoba[1*]; Stephen A. Akinlabi[2]; Esther T. Akinlabi[1]

[1]Department of Mechanical Engineering Science, Faculty of Engineering and the Built Environment, University of Johannesburg, South Africa.

[2] Department of Mechanical and Industrial Engineering Technology, Faculty of Engineering and the Built Environment, University of Johannesburg, South Africa.

Corresponding author*: drfatobasameni@gmail.com

Abstract-Aluminium and its alloys have been successful metal materials used for many applications like commodity roles, automotive and vital structural components in aircrafts. A substantial portion of Al-Fe-Si alloy is also used for manufacturing the packaging foils and sheets for common heat exchanger applications. The present research was aimed at studying the morphology and surface analyses of laser deposited Al-Sn-Si coatings on ASTM A29 steel. These Fe-intermetallic compounds influence the material properties during rapid cooling by laser alloying technique and play a crucial role for the material quality. Thus, it is of considerable technological interest to control the morphology and distribution of these phases in order to eliminate the negative effects on microstructure. A 3 kW continuous wave ytterbium laser system (YLS) attached to a KUKA robot which controls the movement of the alloying process was utilized for the fabrication of the coatings at optimum laser parameters. The fabricated coatings were investigated for its hardness and wear resistance performance. The field emission scanning electron microscope equipped with energy dispersive spectroscopy (SEM/EDS) was used to study the morphology of the fabricated coatings and X-ray diffractometer (XRD) for the identification of the phases present in the coatings. The coatings were free of cracks and pores with homogeneous and refined microstructures. The enhanced hardness and wear resistance performance were attributed to metastable intermetallic compounds formed.
Keywords: Solidification; Al-Sn-Si coating; wear resistance; micro-hardness; crystallization

1. Introduction

The increasing interest in attempting to improve wear, corrosion resistance and hardness of surfaces that are exposed to harsh surroundings and are in contact with abrasives has accelerated the development of several techniques for creating suitable and appropriate protective coatings [1]. Area of failure or degradation for engineering components often begins on the surface. This is because the intensity of

external stress and environmental attacks are often highest at the surface during mechanical and chemical/electrochemical interaction with the surrounding environment [2].

Aluminium based alloy provides good combination of strength and corrosion resistance. They are light in weight, economically viable, amenable for production by various processing techniques and possess high strength and good corrosion resistance. They are widely used in industrial applications due to better tribological properties. Silicon is good in metallic alloys used for casting. This is because it increases the fluidity of the melt, reduces the melting temperature, decreases the contraction associated with solidification and is very cheap as a raw material. Silicon also has a low density (2.34 g cm^{-3}), which may be an advantage in reducing the overall weight of the cast component. Silicon has a very low solubility in aluminium; it therefore precipitates as virtually pure silicon, which is hard and hence improves the abrasion resistance. Tribological properties of Al-Si alloys are affected by the shape and distribution of silicon protection. Because of the excellent tribological properties of Al-Si alloys, they are used in engineering application, especially in plan bearing, internal combustion engine, and hardness increases when silicon is available as coarse polyhedral particles. Al-Si cast alloys have been widely employed to produce automotive components working at ambient and fairly high temperature (up to 200 ºC) due to excellent characteristics such as low-cost manufacturing, excellent castability, high specific strength and recyclability [3, 4]. Al–Sn based alloys are widely used as sliding bearing materials in automobile and shipbuilding industry due to their good compactibility, wear resistance, thermal conductivity, and sliding properties [5]. The alloys also excel in high temperature stability. In these alloy systems, tin is a necessary soft phase in the aluminum matrix. Due to its low modulus, low strength and the excellent anti-welding characteristics with iron, tin phase in Al–Sn bearing materials can provide suitable friction properties and shear surface during sliding [6]. However, literature on Al-Sn-Si alloy coatings through laser surface alloying (LSA) technique is very limited.

LSA modifies the surface morphology and near surface structure of components and its alloys with perfect adhesion to the interface of the bulk steel and the distinctive advantages of the LSA technique for surface modification include the refinement of the grain size because of rapid quench rates and the generation of meta-stable structures with novel properties that are not feasible by competing methods [7, 8]. With optimum laser processing parameters, a reliable coating that is free of cracks and pores can be produced on the matrix. The present study investigates the microhardness property and wear resistance performance of Al-Sn-Si coating on ASTM A29 steel.

2. EXPERIMENTAL DETAILS

2.1. Materials Specifications and Sample Preparation Method

The substrate material used in the present investigation was ASTM A29 steel with the chemical composition (wt%) 0.42 Mn, 0.030 S, 0.010 P, 0.180 C and Balance Fe. The SEM micrograph and XRD spectrum of the ASTM A29 steel are shown in Figure 1. The substrate was cut, and machined into dimensions 75 x 75 x 4 mm^3. Prior to laser treatment, the substrates (ASTM A29 steel) were sandblasted, washed, rinsed in water, cleaned with acetone and dried in hot air before exposure to laser beam to minimize reflection of radiation during laser processing and enhance the absorption of the laser beam radiation. Al (99.9 purity), Sn (99.9% purity) and Si (99.9% purity) reinforcement metallic powders were used as alloying powders mixed in 50:20:30 (A_1) and 60:15:25 (A_2) ratios, respectively, in a shaker mixer

(Turbular T2F; Glenn Mills, Inc.) for 18 hours at a speed of 49 rpm to obtain a homogeneous mixture. The particle shape of the powder used was spherical with 45-90 μm particle sizes. Prior to the characterization of the laser surface alloyed materials, samples were prepared by cutting to rectangles of 15 x 15 mm^2, and cold mounted in clear thermosetting Bakelite resin for optical micrographs and black conductive thermosetting resin for SEM and energy dispersive spectroscopy (EDS) analysis. Specimens for SEM (JSM-7600F; JOEL, Ltd) were prepared by cutting samples in such a way to reveal the transverse section of the coatings. Wear tests were performed on the deposited sample at room temperature using the reciprocating tribometer (CERT UMT-2; Bruker Nano Inc., Campell, CA) under dry reciprocating conditions with continual recording of the dynamic coefficient of friction values. The normal load applied on the samples was 25 N at a frequency of 5 Hz and 2 mm stroke length using tungsten carbide (WC) counter material.

Laser surface alloying was performed using a 3-kW continuous wave (CW) Ytterbium Laser System (YLS) controlled by a KUKA robot which controls the movement of the nozzle head and emitting a Gaussian beam at 1064 nm. The nozzle was fixed at 4 mm from the steel substrate. The admixed powders were fed coaxially by employing a commercial powder feeder instrument equipped with a flow balance to control the powder feed rate. The metallic powder was fed through the off-axes nozzle fitted onto the Ytterbium fibre laser and it was injected simultaneously into a melt pool formed during scanning of the ASTM A29 steel by the laser beam. An argon gas flowing at a rate of 2.5 L/min was used as a shielding gas to prevent oxidation of the sample during laser surface alloying. Overlapping tracks were obtained by overlapping of melt tracks at 50%. To determine the best processing parameters, optimization tests were performed with the laser power of 600 to 900 W and scanning speed varied from 0.6 to 1.0 m/min. The final selection criteria during optimization tests were based on surface having homogeneous layer free of porosity and cracks determined from SEM analysis. The optimum laser parameters used was 750 W power, a beam diameter of 4 mm, gas flow rate of 2.5 L/min, powder flow rate of 2.5 g/min and scanning speeds of 0.6 m/min and 0.8 m/min respectively. X-ray diffraction analyses were carried out utilizing the X'Pert Pro model diffractometer to identify the phases present on the resulted alloyed layer. A Cu Kα radiation fitted on the X'Pert Pro diffractometer set at 40 kV and 20 mA was used to scan in a range between 10^o and 80^o two theta (2θ) with a step size of 0.02^o degrees.

3. Results and Discussion

XRD spectrum of ASTM A29 steel clearly shows a high peak of α-Fe (ferrite phase) at 44.5ºC and low peak of F_3C (cementite) at 67.8ºC. The high α-Fe phase than the peak of F_3C confirms the substrate to be A29 steel. The XRD spectra of admixed powder Al-Sn and alloyed 65Al-15Sn revealed major diffraction peaks with known inter-planar distances. The phases at these peaks are $Al_{13}Fe_4$, Sn, $Al_{0.4}Fe_{0.6}$, and $FeSn_2$ and $Al_{13}Fe_{14}$ as shown in Figure 4. The various phases formed in the laser alloyed samples depend on the laser power, composition of the alloy, and the laser scanning speed. Hard intermetallic phases such as $Al_{0.4}Fe_{0.6}$, $FeSn_2$, and $Al_{13}Fe_4$ were formed in the laser alloyed Al-Sn samples. This may be attributed to the reaction between elemental Al, Sn, and the Fe in the A29 steel substrate.

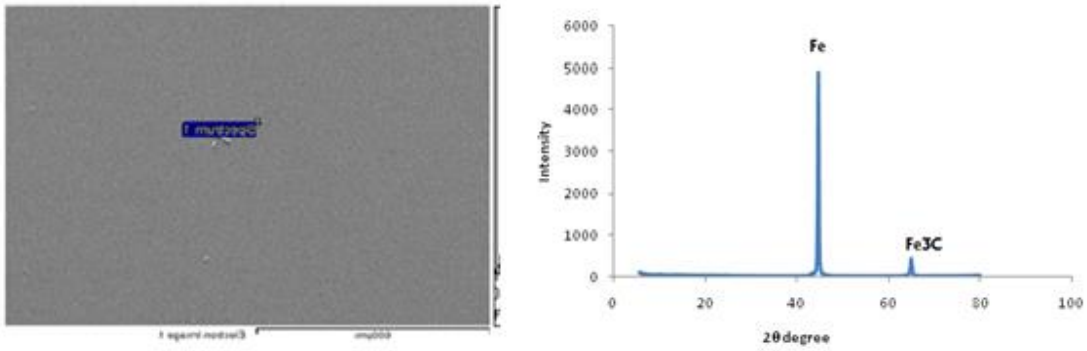

Figure 1: SEM micrograph and XRD spectrum of ASTM A29 steel

3.1 Hardness property of the samples after laser surface alloying.

Microhardness measurements were conducted across the cross section of the deposited hybrid coating tracks (Figure 2), using digital microhardness tester. All the tests were conducted in accordance to the ASTM standards.

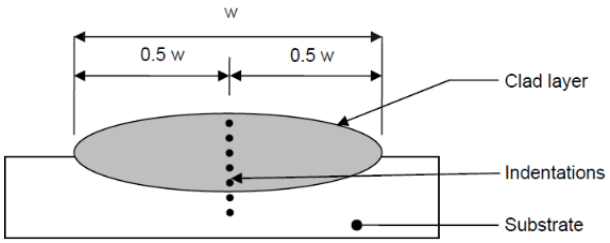

Figure 2: Placement of indentations

The results of the hardness values are shown in Figure 3. The hardness values are highly dependent in the laser scanning speed. It is worthy nothing that as the laser speed increases from 0.6 to 0.8 m/min the hardness values also rise. The high hardness values of the sample at laser speed of 0.8 m/min could be attributed to the smaller grain sizes formed after the laser alloyed process as shown in Figure 5. Increase in hardness value is caused by the obstacle posed to the movement of dislocation by fine grain sizes [9]. Grain size is generally smaller at a faster cooling rate, but the grain size will not reduce further by increasing the cooling rate over a certain rate [10]. Large grain size is the main reason that causes the decrease of hardness and fracture toughness [11].

The lowest and the highest measured microhardness value on the deposited layer across all the 4 samples were found to be 530 and 942 HV respectively. The results showed that the laser alloying process enhances the hardness value of the substrate as shown in Figure 3. The hardness values of 118, 530, 635, 830, and 942 HV were obtained for A29 steel, Al-20Sn-30Si-0.6, Al-20Sn-30Si-0.8, Al-15Sn-25Si-0.6, Al-15Sn-25Si-0.8 respectively. A raise of 85.78 and 87.47% in hardness values above that of the substrate at Al-15Sn-25Si-0.6, and Al-15Sn-25Si-0.8 respectively as shown in Figure 3. This increased hardness values are attributed to the hard phases of iron-aluminium ($Al_{13}Fe4$), iron-tin ($FeSn_2$) formed after the laser alloying process as evident by the XRD spectrum and SEM image shown in Figures 4, 5 and 6. The EDS of the coated sample Al-20Sn-30Si at 0.8 m/min is examined (Figure 6), Fe, Al, Sn, Si, O existed in

the coating. From chemical composition of A29 steel, we deduce that Fe is from the matrix itself, Al, Sn and Si are from main reinforcement powders.

It can also be observed that as the laser speed increases from 0.6 to 0.8 m/min there are smaller grain sizes of the various phases formed. This could be attributed to the fact that increases in laser speed led to faster cooling of the melt pool which resulted in the fine grain sizes as shown in Figure 5. Average grain size increases on decreasing laser scanning speed [11]. The grain size becomes larger when the scanning speed is further decreased. Moreover, increase in number of scan changes to type of heat treatment and produces strain hardening in material causing the grain sizes to be reduced as laser scans increases [12]. In addendum, increase of the scanning speed results in finer microstructure due to the larger cooling rate during solidification [13].

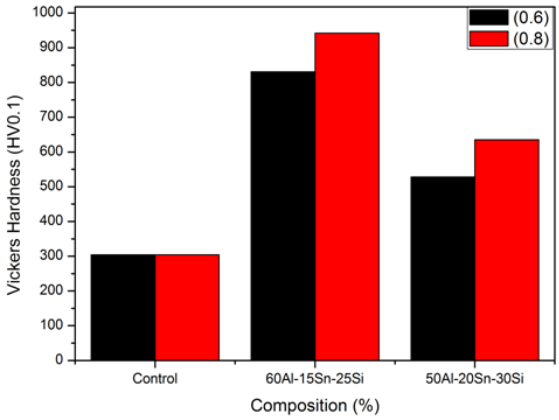

Figure 3: Variation of Hardness values with Al-Sn-Si Coating Compositions

3.2 Microstructural evolution of Al-Sn-Si alloy

The results from the experiment was obtained and it was found there was a presence of α Si phase where the Al-Si alloy depend on the cooling rate and composition of Fe and Si. The Si contents in Si-rich layer increases with increasing Sn content as indicated in 50Al-20Sn-30Si coating. Increasing Sn content from 15 to 20 % caused an increase in nucleation temperature, drop in growth temperature and significant increase in the crystallization temperature of the primary Si [14].

$$L \rightarrow \alpha + \beta(eutectic) \quad (1)$$

L = Liquid phase

α = Predominantly aluminium

β = Predominantly silicon

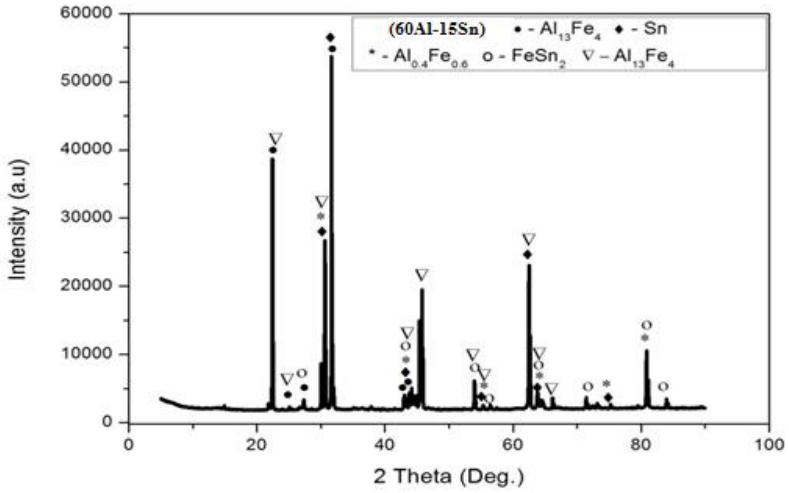

Figure 4: XRD Spectrum of Al-15Sn-25Si Coating at 0.8 m/min scanning speed

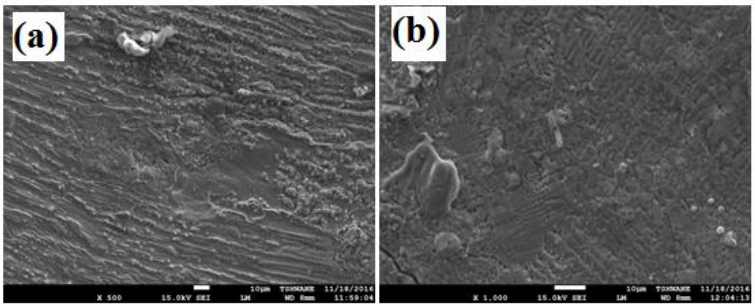

Figure 5: SEM images of Al-15Sn-25Si Coatings at 0.8 m/min (a) x 500 (b) x 1000

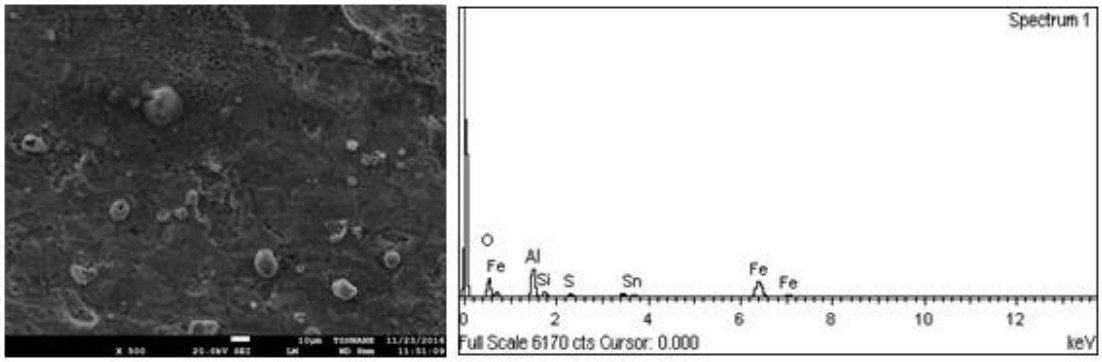

Figure 6: SEM/EDS image of Al-20Sn-30Si Coatings at 0.8 m/min scanning speed

Figure 7 shows the equilibrium phases diagram for the Al-Si system showing metastable extensions of the liquidus and the solidus lines [15]. Al-Si phase diagram is a simple binary eutectic with limited solubility of aluminum in silicon and limited solubility of silicon in aluminum. The solubility of silicon in

aluminum reaches a maximum 1.5 at. % at the eutectic temperature and the solubility of silicon increases with temperature to 0.016% Si at 119^0 C [15].

The authors reported that at higher cooling rates, the system behaves as though the eutectic point is shifted to the higher silicon contents and the eutectic temperature is depressed. The eutectic on this phase diagram contains much more than α and Si and the mixture (α+Si) is expected to be mainly α according to the lever rule at the eutectic temperature. Primary Si forms first, depleting the liquid of Si until eutectic composition is reached and the remaining solidification will follow the eutectic reaction. Most Al-Si alloys always have a near-eutectic composition since it reduces the melting point. Addition of a small quantity of a ternary element like Sn causes modification of the microstructure. The carbon added from the substrate during laser alloying formed carbide to produce Al-Si-C metal matrix composite (MMC) with better thermal expansion performances. Primary Si can be separated from the Al-Si-Sn melt pool and can accumulate to form a Si-rich layer. The content of primary Si in Si-rich layer increases with increasing of Sn content as reported Murray and McAlister [15]. Sn addition tends to enlarge the crystallization temperature range and enhance the separation efficiency.

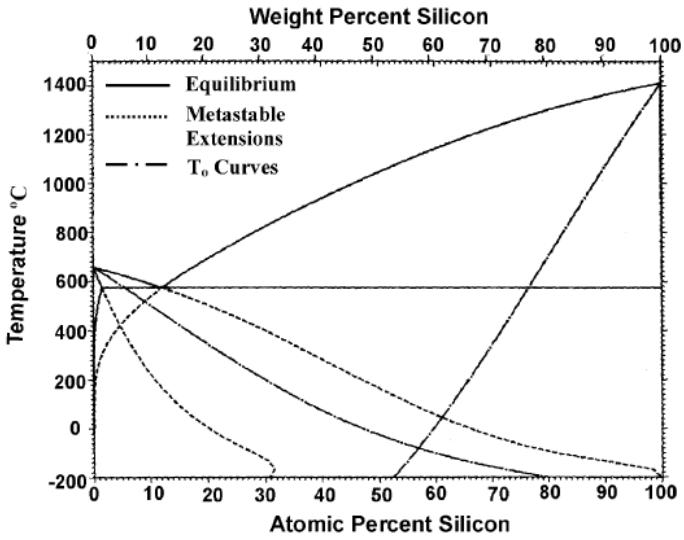

Figure 7: The equilibrium phase diagram for Al-Si system [15].

The results have shown that the use of silicon as an alloying element because of its good properties such as good castability (high fluidity, low shrinkage), the low density of silicon (2.34g/cm) is an advantage as it is able to reduce the overall weight of the component. It also reduces the expansion of Al-Si alloys. Al-Si can be divided into categories: Hypoeutectic (< 12 wt% Si), Eutectic (12-13 wt% Si) and Hypereutectic (14 Wt% Si). Si is the main and most important alloying element of Al-Si alloy. The more Si an alloy contains, the lower is its thermal expansion coefficient. Si is a very hard phase; thus, it contributes significantly to an alloy's wear resistance. Si combines with other elements to improve an alloy's strength and to make alloys heat treatable. Al-Si alloys solidify by a primary precipitation of dendrites. In hypoeutectic Al-Si alloys primary aluminium solidifies dendritically and grows in direction. Dendrites are often drawn having four secondary arms growing around the primary stem at each junction which is true

for cubic structures [15]. The undercooling depends on the cooling rate, the concentration of the alloying element in the melt and the type of the alloying element. It is well established that the undercooling increases with increasing cooling rate and increasing concentration of the alloying element [16].

The cooling rate refinement of eutectic Si-particles has been described based on the surface energy of the Al-Si solid interface [17]. This theory is one of the widely accepted theories for quench modification. The rate of advance of the solidification interface depends on a balance between the rate of heat flow from the liquid to the solid through the interface and the latent heat of fusion released during solidification. The thermal conductivities of Al and Si in their pure form are 205 and 83 W/(mK) respectively, and their latent heats of fusion are 396 and 1411 J/g respectively. Since the difference between the magnitude of the thermal conductivity of pure Al and pure Si and the difference between the magnitude of the latent heat of fusion of pure Al and pure Si are large, Al will solidify much faster than Si. Thus, Al gains a lead during solidification of the eutectic.

3.3 Wear property of the samples after laser surface alloying.

The results indicated that the COF of the control sample decreases with fluctuations in the first 150 s while the ternary coating also exhibited fluctuation in the steady state throughout the sliding time. The fluctuation might be coming from debris formed. The control sample exhibited highest friction coefficient of 0.65. The coefficient of friction drastically reduced with Al-Sn-Si ternary coating. Lack of surface coating is responsible for the poor wear resistance displayed by the control sample with high coefficient of friction. Overall, all the Al-Sn-Si coatings at scanning speed of 0.6 and 0.8 m/min respectively showed remarkable improvements in wear resistance and anti-friction behaviour. Wear resistance is enhanced by increasing hardness according to Archard's equation [18]. Al-15Sn-25Si-0.8 alloy with highest microhardness (920 HV) has the lowest coefficient of friction as shown in Figures 8 and 9. There are two opposite factors influencing the wear rate. First one is the hardness. The higher the hardness, the lower the material removal during the wear test. The second factor affecting the wear rate is the ductility. Material with higher ductility (and usually lower hardness) has higher uniform wear but chipping of bigger particles is limited. Improved wear resistance performance of Al-20Sn alloy was due to high microhardness which increased the load-carrying capacity of the alloy [19]. Wear volume was calculated by measuring the width of the wear scar (transverse to the sliding direction) and the wear depth obtained from the UMT-2 software according to the equation formulated [20]. The wear volume loss graph is shown in Figure 9 indicating that the wear volume losses decreased with increasing laser scanning speed at the same operating conditions. The physical and mechanical properties of surface films are what determine the tribological properties of self-lubrication composites. The chief factor responsible for the excellent tribological properties of these materials is the ability to form surface films during sliding. A new microstructure was induced by the reaction between Fe and Sn which played a fundamental role in the wear process [21]. It is capable of resisting wear which led to a 50% wear reduction. This improvement was attributed to intermetallic $FeSn_2$. This intermetallic $FeSn_2$ is a very hard structure as shown in Figure 4. $FeSn_2$ intermetallic may have contributed to these properties. Enhancement in hardness and compressive strength of Al-matrix composite was due to the presence of iron in the composite. The strengthening mechanism was related to the grain refinement of the matrix, and the formation of $Al_{13}Fe_4$ intermetallic [22].

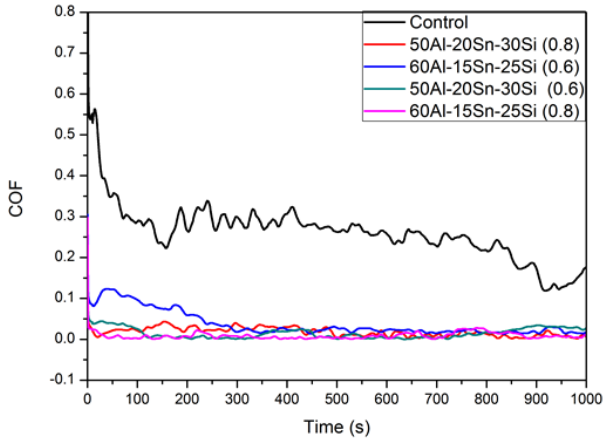

Figure 8: Variation of the Friction Coefficient with Time for the Control and Al-Sn-Si Ternary Coatings.

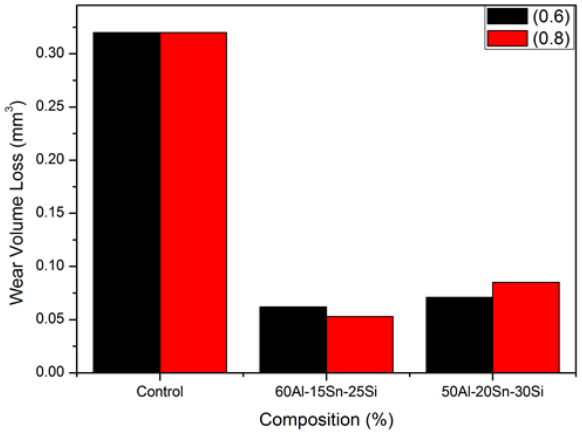

Figure 9: Wear Volume Losses of the Control and Al-Sn-Si Ternary Coatings at 25N Load under Dry Sliding Condition

Moreover, uniform distribution of fine $Al_{13}Fe_4$ intermetallic formed and grain size refinement in aluminium matrix were responsible for enhanced hardness and modulus increase [23-26]. The effects of intermetallic compound on the worn surface of the alloy contribute to the reduction in friction coefficient and wear volume loss. At high temperature reached during wear process, a protective lubricant oxide layer is generated, which prevents the surface from severe damage [27]. The generated oxide provides good layer adhesion which ensures cohesive forces for the contact surfaces [28]. This indicates an outstanding decrease in adhered layer and surface dislocation. Silicon has a very low solubility in aluminium; it therefore precipitates as virtually pure silicon, which is hard and hence improves the abrasion resistance.

4. Conclusion

- Al-Sn-Si coatings were synthesized by continuous wave (CW) Ytterbium Laser System via laser alloying technique to improve the surface property of ASTM A29 steel. The composition

proportion of mixed powders has a great influence on the phase structure of the laser deposited coatings.

- The friction coefficient of coated samples indicated remarkable improvement in wear resistance performance compared to the control sample, with 84.41% and 85.29% reduction in coefficient of friction of Al-15Sn-25Si-0.6, and Al-15Sn-25Si-0.8 respectively. All the ternary coatings samples showed decrease in plastic deformation indicating an outstanding decrease in adhered layer and surface dislocation.
- Enhanced hardness property compared to the unprotected substrate comprised a significant increase in hardness from 118 to 942 HV. A raise of 85.78 and 87.47% in hardness values above that of the substrate at Al-15Sn-25Si-0.6, and Al-15Sn-25Si-0.8 respectively.

References

[1] Dobrzanski, L.A., Bonek, M., Hajduczek, E. & Klimpel, A. 2005. Alloying the X40CrMoV5-1 Steel Surface Layer with Tungsten Carbide by the use of a High-Power Diode Laser. *Applied Surface Science*, **247(1)**, 328-332.

[2] Razavi, R. S. & Gordani, G. R. 2011. Recent Trends in Processing and Degradation of Aluminium Alloys [Online].

[3] Handbook A, New York. ASM International, 1985.

[4] Davies J.R Aluminium and aluminium alloys, ASM international, 1993.

[5] Lepper K, James M, Chashechkina K, Rigneya, D.A. (1997). Sliding behaviour of selected aluminium alloys. *Wear*, **203-204**, 46-56.

[6] Desaki T, Goto Y, Kamiya S. (200). Development of the Aluminium Alloy Bearing with Higher Wear Resistance, *Soc. Autom. Engr. of Japan Rev.* **21**, 321-325.

[7] Kwok, C.T., Cheng, F.T. and Man, H.C. (2006). Cavitation erosion and corrosion behaviour of laser –aluminized mild steel. *Surface and Coatings Technology*. **200**, 3544-3552.

[8] Dobrzanski, L.A., Piec, M., Bonek, M., Jonda, E. and Klimpel, A. (2007). Mechanical and tribological properties of the laser alloyed surface coatings. *Journal of Achievements in Materials and Manufacturing Engineering*. **20(1-2**), 235-238.

[9] Rahman M.J, Sen S.R., Moniruzzaman M. and Shorowordi K.M. (2009). Morphology and properties of electrodeposited Zn-Ni alloy coatings on mild steel, *J. Mech. Eng. Trans. Mech. Eng. Div. Inst. Eng*. **40**, 9-12.

[10] Liu X., Warren A.P., Nuhfer N.T., Rollett A.D., Coffey K.R. and Barmak K. (2014). Comparison of Crystal Orientation Mapping-Based and Image Measurement of Grain Size Distribution in a Thin Aluminium Film. *Acta Materialia,* **79**, 138-145.

[11] Shuai C. Feng, P. Zhang L. Gao C. Hu H. Peng S. and Min A. (2013). Correlation between Properties and Microstructure of Laser Sintered Porous β-TriCalcium Phosphate Bone Scaffolds, *Sci. Technol. Adv. Mater*. **14**, 1-10.

[12] Akinlabi E.T. and Akinlabi S.A. (2012). Effect of Heat Input on the Properties of Dissimilar Friction Stir Welds of Aluminium and Copper. *Amer. J. Mater. Sci*. **2,** 147-152.

[13] Gong X. Lydon J. Cooper K. Chou K. (2014b). Beam Speed Effects on Ti-6Al-4V Microstructures in Electron Beam Additive Manufacturing, *J. Mater. Res*. **29**, 1951-1959.

[14] Zou Q.C. Jie J.C. Dong Y. Li T.J. Effect of Sn addition on the electromagnetic separation of primary Si from Al-30Si alloy during solidification. 8th International Conference on Electromagnetic Processing of Materials, Oct 2015, Cannes, France. EPM2015.

[15] Murray J.L. and McAlister A.J. (1984). Alloy Phase Diagrams, *Bull.* **5**, 74-84.

[16] Fredriksson H. and Åkerlind U. (2012). Solidification and Crystallization Processing in Metals and Alloys, John Wiley & Sons Ltd., Chichester, 2012.
[17] Makhlouf, M. and Guthy H. (2001*). Journal of Light Metals*, **1**, 199-218.
[18] Archad A. (1953). Contact and Rubbing of Flat Surfaces. *J. Appl. Phys*, **24**, 981-988.
[19] Liu X., Zeng M.Q., Ma Y. Zhu M. (2008). Wear behaviour of Al-Sn alloys with different distribution of Sn dispersoids manipulated by mechanical alloying and sintering. *Wear*, **265,** 1857-1863.
[20] Qu J. and Truhan J.J. (2006). An efficient method for accurately determining wear volumes of sliders with non-flat wear scars and compound curvatures. *Wear*, **261**, 848–855.

[21] Kossowsky R. and Singhal S.C. (2012). Surface Engineering, *Surface Mod. Mater. Technol. Eng*. **764**, 1-8.

[22] Fathy A., El-Kady O. and Mohammed M.M.M. (2015). Effect of iron addition on microstructure, mechanical and magnetic properties of Al-matrix composite produced by powder metallurgy route. *Trans. Non-Ferrous Met. Soc. China*, **25**, 46-53.
[23] Lee I.S. Kao P.W. and Ho N.J. (2008). Microstructure and mechanical properties of Al-Fe in-situ nanocomposite produced by friction stir processing. *Intermetallics*, **16**, 1104-1108.
[24] Makhatha, M.E., Fatoba, O.S. and Akinlabi, E.T. (2017). Effects of rapid solidification on the microstructure and surface analyses of laser-deposited Al-Sn coatings on AISI 1015 steel. *Int J Adv Manuf Technol.* 1-15. https://doi.org/10.1007/s00170-017-0876-y

[25] Fatoba O.S., Akinlabi E.T. and Makhatha M.E. (2017). Effect of silicon on the microstructure, mechanical and surface properties of laser metal deposition Al-Si based coatings, Fiber Laser, Dr. Subbarayan Sivasankaran (Ed.), InTech, http://dx.doi.org/10.5772/intechopen.71698

[26] Fatoba O.S. Akinlabi E.T. and Makhatha M.E. (2017). Effect of Process Parameters on the Microstructure and Tribological Property of Zn-Sn-Ti Coatings on AISI 1015 Steel: Laser Alloying Technique. *International Journal of Surface Science and Engineering.* **11 (6),** 489-511.

[27] Zhu M. and Gao Y. (2000). Improvement of the wear behaviour of Al-Pb alloys by mechanical alloying. *Wear*, **242**, 47-53.
[28] Su Y.L. and Kao W.H. (2003). Tribological behaviour and wear mechanism of MoS_2-Cr coatings sliding against various counter-bodies. *Tribol. Int.* **36**, 11-26.